High-resolution electron-momentum spectroscopy of argon: Validation of technique and approximations

M. J. Brunger and I. E. McCarthy
Department of Physics, The Flinders University of South Australia, G.P.O. Box 2100, Adelaide 5001, Australia

E. Weigold
Research School of Physical Sciences and Engineering, Institute of Advanced Studies, Australian National University, Canberra, Australian Capital Territory 0200, Australia

(Received 18 June 1998)

$(e,2e)$ cross sections for argon have been measured for binding energies in the valence regime of the ion at energies of 500, 1000, 1500, and 1800 eV. The kinematic arrangement is noncoplanar symmetric. Cross sections are relatively normalized for each energy. The assumptions of electron-momentum spectroscopy are verified in detail. The distorted-wave impulse approximation with Hartree-Fock orbitals describes the data within experimental error. It gives the correct inner valence *s* orbital manifold cross section relative to the outer valence *p* manifold at all energies. Orbital manifolds of ion states are identified, within which cross-section ratios are independent of energy and recoil momentum. Spectroscopic factors are defined by the ratio of the cross section for an ion state to the cross section for the orbital manifold. The spectroscopic sum rule is verified. [S1050-2947(99)03802-0]

PACS number(s): 34.80.Dp, 34.80.Nz

I. INTRODUCTION

Electron-momentum spectroscopy (EMS) depends on the high-energy and high-momentum-transfer $(e,2e)$ reaction, a kinematically complete observation of the ionization of an atomic, molecular, or solid target by an electron beam of energy E_0. Electronic states i of the residual ion are resolved in binding energy ϵ_i, which is the eigenvalue of the state with reversed sign. For each state the differential cross section is measured as a function of ion recoil momentum $\mathbf{p}$, producing a momentum profile. In the experiment relative cross sections are measured at a given energy for the observed states i, but one overall absolute normalization is not determined. In order to scan momentum from zero to several atomic units it is convenient to arrange the experiment so that only one kinematic quantity is varied. For gas targets this is normally the out-of-plane azimuthal angle $\pi-\phi$ between the directions of the emergent electrons in noncoplanar symmetric kinematics, where the energies of the electrons are equal and fixed and the polar angles are each 45°. This arrangement maximizes the momentum transfer from the scattered to the ejected electron. The binding energy ϵ is scanned by varying E_0.

The simple interpretation of the experiment in terms of the independent-particle model is that at sufficiently high energy and momentum transfer the elementary electron-electron collision is impulsive, so that the observed recoil momentum $\mathbf{p}$ is equal and opposite to the momentum $\mathbf{q}$ of the target electron at the collision instant. The momentum profile is therefore the momentum density of the target electron, given by the absolute square of its orbital.

The experiment by Weigold, Hood, and Teubner [1] in 1973 observed the valence structure of the argon atom. Momentum profiles were very close to the $3p$ and $3s$ Hartree-Fock forms predicted by the independent-particle model, but more states were observed than the two predicted in this interpretation. The lowest-energy ion state at 15.76 eV exhibited the $3p$ momentum profile but the others, between 29 and 43 eV, had similar profiles close to the $3s$ form.

The independent-particle interpretation was refined by Furness and McCarthy [2], who considered a configuration-interaction expansion of the ion states. The momentum profile classifies the ion states into orbital manifolds. In the $3s$ manifold, for example, the reaction observes the $3s$-hole configuration, which consists of a hole in the $3s$ orbital of the target ground state. Relative cross sections for states of the manifold give the relative probability of finding the one-hole configuration in the expansion. The probabilities, normalized to a total probability 1, are the spectroscopic factors. EMS therefore not only observes orbitals, but spectroscopic factors specifying electron correlations.

It is essential to emphasize that the experiment contains internal verification of the interpretation. First, the momentum profiles for states in the same orbital manifold must have the same shape. The structure interpretation contains no reference to the experimental conditions. Therefore the spectroscopic factors must be independent of the incident energy E_0 and of the absolute recoil momentum p. If a sufficient theoretical understanding of the reaction is achieved to predict the orbital momentum-profile shape, then the spectroscopic factor S_i^α for the state i of the manifold α is the ratio of the experimental profile to the orbital profile. Spectroscopic factors, thus determined for different orbital manifolds, must sum to the same value, normalized to 1, for each manifold.

Since 1973 EMS has been verified by a large body of data within various limits of accuracy [3–5]. Nevertheless doubts have been raised from time to time, mainly based on the very different cross-section ratios for states of the same orbital manifold [6] observed by another kinematically complete ionization reaction, photoionization at x-ray energies x-ray

photoelectron spectroscopy (XPS). Argon $3s$ is an excellent example of this. The reason for the difference is simple. The two-body final-state kinematics of XPS constrains the recoil momentum to be of order 10 a.u., so that the relevant bound-state momentum components are far outside the 0–3-a.u. range for which valence orbitals have significant values. The existence of a finite cross section therefore depends on details of electron correlations, represented by excited configurations in the target ground state and the observed ion state, and not just on the one-hole configuration as does EMS. An excellent understanding of the situation was achieved by Amusia and Kheifets [7], and confirmed for the argon $3s$ manifold by a many-body perturbation calculation [8], which agreed with experiment both for EMS and XPS.

The purpose of the present work is to show, using the example of argon, that a sufficient theoretical understanding of EMS can be achieved to obtain detailed agreement with a high-quality experiment by a simple *ab initio* calculation at a wide range of incident energies. This understanding, described in Sec. III, confirms the spectroscopic-factor interpretation. Experimental confirmation is provided by the energy and momentum independence of the spectroscopic factors.

In the next section we provide a brief description of the present experiment. A discussion of the theory of EMS is found in Sec. III, while our results and a discussion of them are given in Sec. IV. Finally some conclusions are drawn in Sec. V.

II. DESCRIPTION OF THE EXPERIMENT

The present experiments were conducted with a noncoplanar symmetric electron coincidence spectrometer. This electron-coincidence spectrometer and the techniques used in the present investigation have been described at length previously by McCarthy and Weigold [3] (to which the interested reader is referred for more information), and so we do not go into further detail here. We note, however, that there have been three major developments to the coincidence spectrometer since the description provided in McCarthy and Weigold.

(a) The computer hardware and operating system (data handling, processing, and storage) have been upgraded.

(b) The collision region is now differentially pumped.

(c) An electron monochromator (for the incident electrons) has been brought on line, an advance that has considerably improved the achievable coincidence energy resolution.

A full discussion of these developments [(a)–(c)] is not strictly relevant to this paper and can be found elsewhere [9].

The high-purity argon is emitted into the target chamber through a capillary tube, the leak rate being controlled by a variable leak valve. The collision region is surrounded by a chamber pumped by a 700-$\mathrm{l\,s^{-1}}$ diffusion pump. Apertures and slits are cut in the collision chamber for the incident beam and ejected electrons. The differentially pumped collision region makes it possible to increase the target gas density by a factor of about 3 while keeping the background pressure in the spectrometer below 10^{-5} Torr. This was important as it allowed us to maintain workable coincidence count rate levels, even with the smaller electron beam current output from the $(e,2e)$ monochromator (typically 30 μA) compared to that of a normal electron gun [3]. The coincident energy resolution of the present measurements was in the range 0.55–0.61 eV [full width at half maximum (FWHM)], the actual value depending on the beam energy under study. The components that contribute to this overall coincident energy resolution are due to the energy spread of the incident electron beam (typically ~0.35–0.44 eV FWHM), and the resolution of each electron analyzer (typically each is ~0.3 eV FWHM). Note the components are added in quadrature to determine the overall resolution. The angular resolution was typically 1.2° (FWHM). Noncoplanar symmetric kinematics was employed, that is, the outgoing electron energies E_A and E_B are equal, the two emitted electrons making equal polar angles $\theta = 45°$ with respect to the direction of the incident electrons. The total energy (E), $E_0 - \epsilon_i = E_A + E_B$, was, respectively, either 500, 1000, 1500, or 1800 eV. The recoil momentum $\mathbf{p}$ was varied by varying the out-of-plane azimuthal angle ϕ over the angular range 0°–30°. Binding-energy spectra were taken at each out-of-plane azimuthal angle over the range $\epsilon_i = 13-45$ eV using the binning mode [3].

III. THEORY OF EMS

The object of a theoretical description of the $(e,2e)$ reaction in the EMS kinematic region is to find an *ab initio* method of calculation that obtains detailed agreement with experiment. This is not the same as a general solution of the corresponding three-body problem, which still defies our efforts, in spite of the success at low energy of the convergent-close-coupling method [10]. The EMS kinematic region is in fact chosen so that the reaction calculation is relatively simple and exposes the structure information to detailed analysis.

We denote the measured momenta of the incident and two emergent electrons by $\mathbf{k}_0$, $\mathbf{k}_A$, and $\mathbf{k}_B$. The differential cross section for the reaction is, in atomic units,

$$\frac{d^5\sigma}{d\Omega_A d\Omega_B dE_A} = (2\pi)^4 \frac{k_A k_B}{k_0} \sum_{\mathrm{av}} |\langle \mathbf{k}_A \mathbf{k}_B i | T | 0 \mathbf{k}_0 \rangle|^2, \quad (1)$$

where the target ground state is 0 and the observed ion state is i. The operator T describes the whole collision. Σ_{av} denotes a sum and average over final and initial degenerate states, which are magnetic and spin states for an atomic target.

Before making a detailed approximation for T we make the binary-encounter approximation. This assumes that T does not depend explicitly on the coordinates of the residual ion, so that it commutes with the ion state vector. Introducing a complete set of target-electron-momentum states $|\mathbf{q}\rangle$, the ionization amplitude becomes

$$\langle \mathbf{k}_A \mathbf{k}_B i | T | 0 \mathbf{k}_0 \rangle = \int d^3q \langle \mathbf{k}_A \mathbf{k}_B | T | \mathbf{q} \mathbf{k}_0 \rangle \langle \mathbf{q} i | 0 \rangle. \quad (2)$$

This form exposes all the structure information in the structure amplitude $\langle \mathbf{q}i|0\rangle$. The ionization amplitude is a reaction transform of the structure amplitude, where the transform kernel is the two-electron amplitude $\langle \mathbf{k}_A\mathbf{k}_B|T|\mathbf{q}\mathbf{k}_0\rangle$. Independent of the reaction details, this form is subject to experimental verification, since overall multiplicative factors in the structure amplitude, for example, spectroscopic factors in the corresponding structure approximation, simply multiply the ionization amplitude and can be determined, up to a normalization, by comparing cross sections.

The simplest approximation for the two-electron amplitude assumes that the kinetic energies of the external electrons are so high that the effective potentials due to the residual systems are negligible in comparison. The electron-electron interaction, represented by the t matrix [11], is responsible for the reaction and cannot be neglected. This is the impulse approximation, which is the first term of the multiple-scattering series [12]

$$\langle \mathbf{k}_A\mathbf{k}_B|T|\mathbf{q}\mathbf{k}_0\rangle = A\langle \tfrac{1}{2}(\mathbf{k}_A-\mathbf{k}_B)|t(E)|\tfrac{1}{2}(\mathbf{k}_0-\mathbf{q})\rangle\,\delta(\mathbf{q}+\mathbf{p}), \tag{3}$$

where the observed recoil momentum is

$$\mathbf{p}=\mathbf{k}_0-\mathbf{k}_A-\mathbf{k}_B\,, \tag{4}$$

and the t matrix is half off shell [3] at the energy E corresponding to the free-electron final state. The antisymmetrization operator is A. The impulse approximation is in fact the formal expression of the simplistic interpretation that the recoil momentum $\mathbf{p}$ is equal and opposite to the target-electron momentum $\mathbf{q}$. It is very closely valid at $E_0=20\,\mathrm{keV}$, where it has been tested for argon in the spectrometer used for EMS of solids [13].

For atomic and molecular targets the need to resolve electronic states i makes incident energies in the 1-keV range an appropriate choice. For atoms the effect of the residual systems on the external electrons may be represented by central potentials, whose first-order term is the static-exchange potential. Second-order terms have been shown to be negligible within experimental error [14]. The external electron of momentum $\mathbf{k}$ is represented by an elastic-scattering function $\chi^{(\pm)}(\mathbf{k})$ with boundary conditions appropriate to ingoing or outgoing electrons. The resulting form is the distorted-wave impulse approximation (DWIA), which is tested in the present analysis. The two-electron amplitude is Eq. (3), but the structure amplitude in Eq. (2) is replaced by

$$\int d^3k_1\int d^3k_2\int d^3k_3\langle \chi^{(-)}(\mathbf{k}_A)|\mathbf{k}_1\rangle\langle \chi^{(-)}(\mathbf{k}_B)|\mathbf{k}_2\rangle \times\langle \mathbf{k}_3|\chi^{(+)}(\mathbf{k}_0)\rangle\langle \mathbf{q}i|0\rangle, \tag{5}$$

where

$$\mathbf{q}=\mathbf{k}_1+\mathbf{k}_2-\mathbf{k}_3\,. \tag{6}$$

The form (5) is written to display the structure amplitude explicitly. The computational form is quite simple, but will be left until the approximation for the structure amplitude has been discussed.

Because of the integration over the ion coordinates the structure amplitude $\langle \mathbf{q}i|0\rangle$ is a one-electron function, the quasiparticle or Dyson orbital. We consider the orbital manifold α, choosing a reference set α, β of theoretical orbitals, calculated in a potential $U+v$. where U is the electrostatic potential and the reference potential v is chosen appropriately.

It is possible formally to select one hole from the many-body problem for the target and write the Schrödinger equation for the ion as a one-electron equation, the quasiparticle equation [15], whose momentum-space representation is

$$\langle \mathbf{q}i|[\tfrac{1}{2}p^2+U+w(\epsilon_i^\alpha)+\epsilon_i^\alpha]|0\rangle=0,\quad i\in\alpha \tag{7}$$

where the complexities of the problem are contained in the nonlocal and explicitly energy-dependent operator $w(\epsilon_i^\alpha)$, which may be called the optical potential. For the Hartree-Fock approximation $w(\epsilon_i^\alpha)$ is the exchange potential. In the Kohn-Sham density-functional approximation [16] it is the exchange-correlation potential, where correlations are defined with respect to the reference set of orbitals. Alternatively, it may be approximated perturbatively [17].

We obtain the integral-equation form of Eq. (7) by expanding $\langle \mathbf{q}i|0\rangle$ in the spectral representation of the reference-orbital Hamiltonian $\frac{1}{2}p^2+U+v$ and using its inverse, defined by Eq. (7).

$$\langle \mathbf{q}i|0\rangle=\langle \mathbf{q}|\alpha\rangle\langle \alpha i|0\rangle-\sum_{\beta\neq\alpha}\langle \mathbf{q}|\beta\rangle\frac{1}{\epsilon_i^\alpha-\epsilon^\beta} \times\langle \beta i|w(\epsilon_i^\alpha)-v|0\rangle,\quad i\in\alpha. \tag{8}$$

For the structure amplitude $\langle \mathbf{q}i|0\rangle$ we make the weak-coupling approximation by choosing the reference potential v to approximate $w(\epsilon_i^\alpha)$ as closely as possible, thereby making the second term of Eq. (8) very small on the scale of $\langle \mathbf{q}|\alpha\rangle$ for values of q in the range 0–3 a.u. This definition of the reference potential produces a special reference orbital ϕ^α, which we call the normalized Dyson orbital of the manifold α. It is the orbital defined by the reaction. The one-hole state is defined by an electron of the target ground state in this orbital. The weak-coupling approximation to the structure amplitude is

$$\langle \mathbf{q}i|0\rangle=\langle \mathbf{q}|\phi^\alpha\rangle\langle \phi^\alpha i|0\rangle. \tag{9}$$

It takes the form of the normalized Dyson orbital multiplied by the spectroscopic amplitude, whose square is the spectroscopic factor

$$S_i^\alpha=|\langle \phi^\alpha i|0\rangle|^2. \tag{10}$$

The sum rule for spectroscopic factors in the manifold α is obtained from the completeness relation for i and the normalization of 0 and ϕ^α,

$$\sum_{i\in\alpha}\langle 0|i\phi^\alpha\rangle\langle \phi^\alpha i|0\rangle=1. \tag{11}$$

The approximation that we use for the ionization reaction is the DWIA, whose name implies the weak-coupling approximation for the structure amplitude. In noncoplanar symmetric kinematics

TABLE I. Spectroscopic factors for $^2P^o$ manifold states at $\phi=0°$ and 10°, and $E=500$, 1000, 1500, and 1800 eV. The momenta (p) in a.u. corresponding to $\phi=0°$ or 10° are indicated in square brackets for the dominant transition. The state classifications are due to McCarthy *et al.* [19] and Svensson *et al.* [6].

	E (eV)		500		1000		1500		1800	
Peak No.	ϵ_i (ev)	Final state	$\phi=0°$ [0.086]	$\phi=10°$ [0.537]	$\phi=0°$ [0.069]	$\phi=10°$ [0.751]	$\phi=0°$ [0.059]	$\phi=10°$ [0.917]	$\phi=0$ [0.055]	$\phi=10°$ [1.004]
1	15.76	$3s^23p^5\,^2P^o$	0.95 [1]	0.95 [1]	0.96 [1]	0.95 [1]	0.94 [1]	0.95 [1]	0.93 [1]	0.95 [1]
4	35.60	$3s^23p^4(^3P)4p\,^2P^o$	0.01 [1]	0.01 [1]	0.01 [1]	0.01 [1]	0.01 [1]	0.01 [1]	0.02 [1]	0.01 [1]
6	37.15	$3s^23p^4(^1D)4p\,^2P^o$	0.03 [1]	0.03 [1]	0.025 [10]	0.03 [1]	0.04 [1]	0.03 [1]	0.04 [1]	0.03 [1]
8	39.56	$3s^23p^4(^1S)4p\,^2P^o$	0.01 [1]	0.01 [1]	0.005 [5]	0.01 [1]	0.02 [1]	0.01 [1]	0.01 [1]	0.01 [1]

$$\frac{d^5\sigma}{d\Omega_A d\Omega_B dE_A} = KS_i^\alpha \sum_m |\langle \chi^{(-)}(\mathbf{k}_A)\chi^{(-)}(\mathbf{k}_B)|\phi^\alpha \chi^{(+)}(\mathbf{k}_0)\rangle|^2. \tag{12}$$

The summation is over magnetic degeneracies. All the kinematic and electron-electron collision factors have an imperceptible energy dependence and are summarized in the kinematic constant K, which is irrelevant since an overall normalization is not determined by the experiment. The approximation takes the form of a distorted momentum profile multiplied by a spectroscopic factor. It defines the normalized Dyson orbital for each manifold. These orbitals may be extracted from the experimental data by a fitting procedure [18], which constrains them to be orthogonal. Alternatively an *ab initio* calculation postulates a reference potential v, which should describe the data within experimental error.

The experimental verification of the approximation (12) depends on the following criteria.

(1) The distorted-wave momentum profile at a particular E must have the same shape for all the states of each orbital manifold.

(2) The cross-section ratios for all the states of the manifold must be independent of E and p.

(3) If enough states have been observed to exhaust each orbital manifold, then the spectroscopic factors, determined by the ratio of the experimental and calculated profiles, must sum to the same number for each manifold. The number is normalized to 1 for a chosen manifold.

IV. RESULTS AND DISCUSSION

The binding-energy spectrum of argon in the region $\epsilon_i = 13-45$ eV is shown in Fig. 1 for a total energy of 1000 eV and at $\phi=0°$. The spectrum presented in Fig. 1 is considerably better resolved than those published in earlier works [1, 19–23], reflecting the higher coincident energy resolution of this investigation. In addition, the statistical quality of the current study is improved over that obtained in the earlier work. The advantages of this are manifest. First, overlap between the various states due to the wings of the instrumental resolution function is minimized. This aids the fitting process in that uniqueness problems with the derived parameters are negated. Thus this ensures that possible distortions in the derived momentum distributions (MDs), due to the deconvolution, are avoided. The improved statistical quality of our data also aids in the deconvolution process. Indicative recoil momenta, corresponding to the out-of-plane azimuthal angles $\phi=0°$ and 10°, depend on the energy and also somewhat on the binding energy. At 1000 eV and $\phi=0°$ the momentum p ranges from 0.069 a.u. at the binding energy of the first peak ($\epsilon_i=15.76$ eV) to 0.118 a.u. at the binding

TABLE II. Spectroscopic factors for ^2S manifold states at $\phi=0°$ and 10°, and $E=500$, 1000, 1500, and 1800 eV. The momenta (p) corresponding to $\phi=0°$ or 10° are indicated in square brackets for the dominant transition. The state classifications are due to McCarthy *et al.* [19] and Svensson *et al.* [6].

	E (eV)		500		1000		1500		1800	
Peak No.	ϵ_i (eV)	Final state	$\phi=0°$ [0.164]	$\phi=10°$ [0.553]	$\phi=0°$ [0.118]	$\phi=10°$ [0.757]	$\phi=0°$ [0.099]	$\phi=10°$ [0.921]	$\phi=0°$ [0.092]	$\phi=10°$ [1.007]
2	29.24	$3s3p^6\,^2S$	0.55 [1]	0.55 [2]	0.55 [1]	0.54 [2]	0.55 [1]	0.56 [2]	0.55 [1]	0.54 [2]
5	36.52	$3s^23p^4(^1S)4s\,^2S$	0.02 [1]	0.02 [1]	0.02 [1]	0.02 [1]	0.02 [1]	0.02 [1]	0.02 [1]	0.02 [1]
7	38.60	$3s^23p^4(^1D)3d\,^2S$	0.16 [1]	0.16 [2]	0.16 [1]	0.16 [2]	0.15 [1]	0.15 [2]	0.16 [1]	0.17 [2]
9	41.21	$3s^23p^4(^1D)4d\,^2S$	0.08 [1]	0.08 [2]	0.08 [1]	0.09 [2]	0.09 [1]	0.08 [2]	0.08 [1]	0.07 [2]
10	42.67	$3s^23p^4(^1D)5d\,^2S$	0.05 [1]	0.05 [1]	0.05 [1]	0.06 [1]	0.05 [1]	0.05 [1]	0.05 [1]	0.05 [1]
11	43.4	$3s^23p^4(^1D)6d\,^2S$	0.03 [1]	0.03 [1]	0.03 [1]	0.02 [1]	0.03 [1]	0.03 [1]	0.03 [1]	0.04 [1]
12	44.0	$3s^23p^4(^1D)7d,\ 8d\,^2S$	0.015 [5]	0.015 [5]	0.014 [5]	0.014 [5]	0.015 [5]	0.014 [5]	0.014 [5]	0.014 [5]
13	44.6	Rydberg series	0.015 [5]	0.015 [5]	0.016 [5]	0.016 [5]	0.015 [5]	0.016 [5]	0.016 [5]	0.016 [5]

[a]Allows for missing ~8% intensity in the continuum ($\epsilon>45$ eV) as verified in this study.

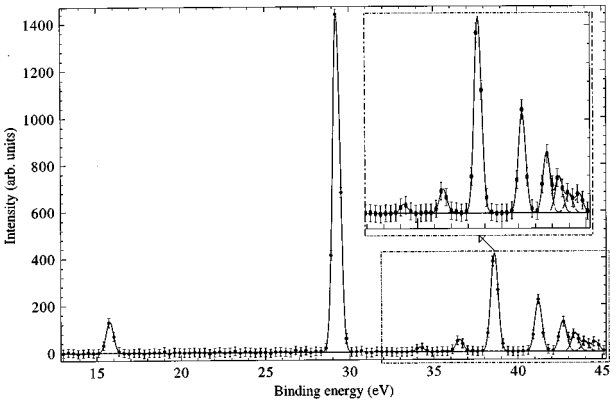

FIG. 1. 1000-eV noncoplanar symmetric EMS binding-energy spectrum at $\phi=0°$. The curves show the fitted spectrum using the known coincident energy resolution. Note that in the inset we have, for $\epsilon_i>32$ eV, scaled the data by a factor of 2 to better indicate the observed structure.

energy of the main $3s^{-1}$ satellite ($\epsilon_i=29.24$ eV). The corresponding momenta for $\phi=10°$ are 0.751 and 0.757 a.u., respectively. At 1800 eV and $\phi=0°$ the momentum ranges from 0.055 a.u. at $\epsilon_i=15.76$ eV to 0.092 a.u. at $\epsilon_i=29.24$ eV. The corresponding momenta in this case for $\phi=10°$ are 1.004 and 1.007 a.u., respectively.

Thirteen Gaussian peaks were fitted to the binding-energy spectra measured in this study. In the fitting procedure the peak positions are given by independent photoelectron spectroscopy (PES) measurements [6] and accurate spectroscopy tables [24] and their widths are equal to the measured energy resolution. Therefore the peak height is the only parameter remaining to be fitted. A few points per peak suffice to do this. Four states (peaks 1, 4, 6, and 8) had significantly more intensity at $\phi=10°$ compared to that measured at $\phi=0°$, and thus belong to the $^2P^o$ manifold. A further eight of these peaks (peaks 2, 5, 7, 9–14) had significantly more intensity at $\phi=0°$ compared to that measured at $\phi=10°$, and thus belong to the $^2S^e$ manifold. The classifications for these peaks of $^2P^o$ and $^2S^e$ symmetry and their experimental binding energies, which are entirely consistent with the earlier EMS result of McCarthy *et al.* [19] and the PES result of Svensson *et al.* [6], are given in Tables I and II. The thirteenth peak, at $\epsilon_i=34.20$ eV, does not correspond to a final state with $^2P^o$ or $^2S^e$ symmetry which must occur if, respectively, a $3p$ or $3s$ electron in the target-Hartree-Fock approximation (THFA) is emitted. Moore [24] noted a state of

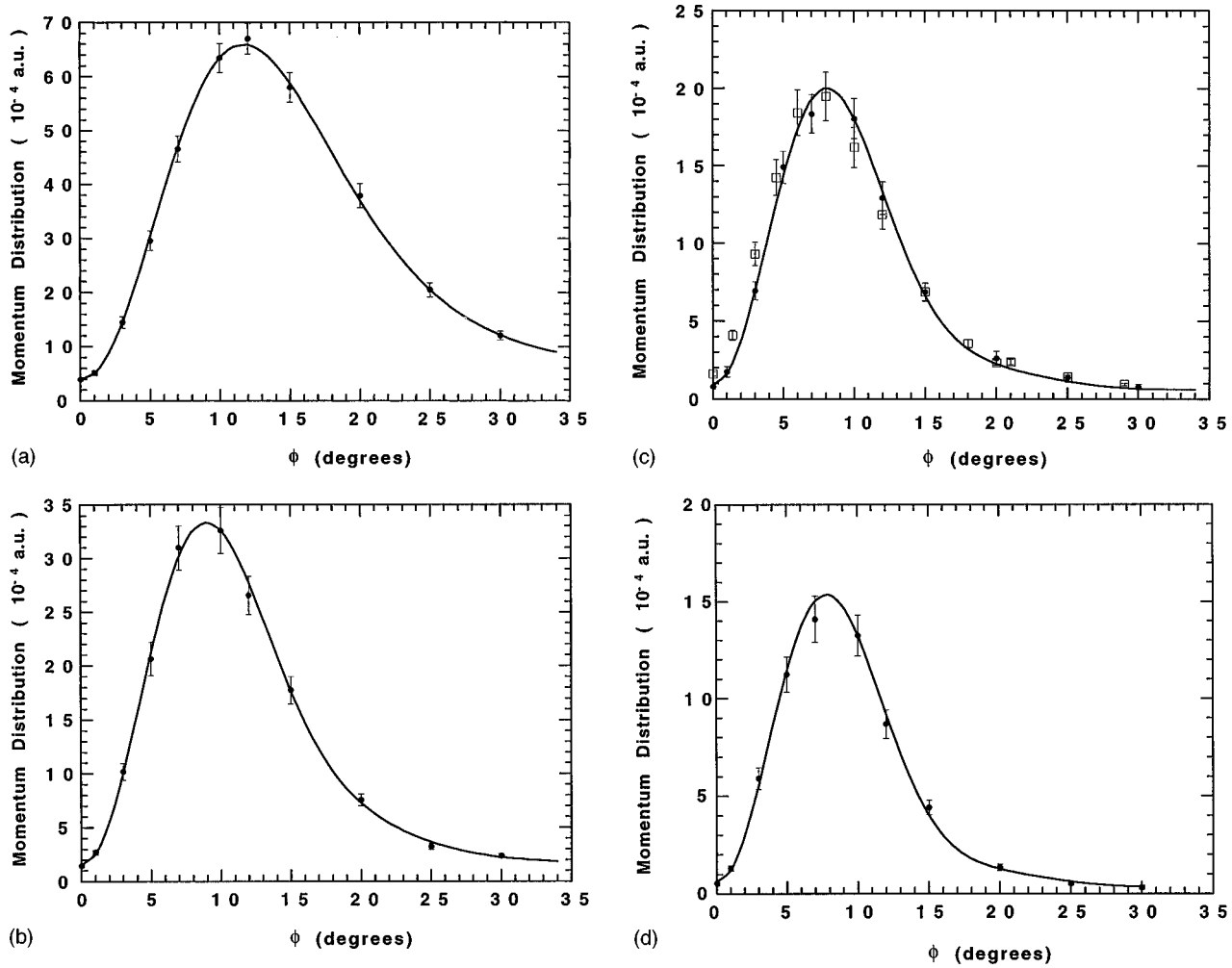

FIG. 2. Noncoplanar symmetric momentum distributions for the ground $3p$ state transition ($\epsilon_i=15.76$ eV) at (a) 500, (b) 1000, (c) 1500, and (d) 1800 eV. The present data (●), 0.95×DWIA (-), and the earlier result of McCarthy *et al.* (□) are plotted. Note the present data are normalized to 0.95×DWIA at $\phi=10°$.

$^2D^e$ symmetry at 34.20 eV in Ar^+, for which she assigned the configuration $3s^2 3p^4(^1D)4s\,^2D$. Such a state can only be excited if there are suitable *d*-wave correlations in the ground state, as was specifically demonstrated in the calculations of Mitroy *et al.* [25]. This satellite was observed in EMS by McCarthy *et al.* [19].

Binding-energy spectra similar to that shown in Fig. 1 were also taken over the range of out-of-plane azimuthal angles $\phi = 0° - 30°$ and at each total energy. Note that for the present kinematical arrangement ϕ and momentum p are simply related through the transformation

$$p = \left[(2k_A \cos\theta - k_0)^2 + 4k_A^2 \sin^2\theta \sin^2\frac{\phi}{2} \right]^{1/2}. \quad (13)$$

Since each part of each spectrum at every angle was scanned sequentially for an equal time, each run consisting of many scans, the spectra can be used to obtain the cross sections to selected final ion states relative to each other as a function of ϕ, or the recoil momentum p.

The noncoplanar $(e,2e)$ cross sections for the ground $3p^{-1}$ transition at $\epsilon_i = 15.76$ eV are given in Fig. 2 at (a) 500, (b) 1000, (c) 1500, and (d) 1800 eV. The solid line is the DWIA cross section obtained from Eq. (12) with the finite angular (momentum) resolution folded in. The $3p$ Hartree-Fock orbital of Clementi and Roetti [26] was used in the calculations to approximate the Dyson orbital. The measured cross sections are relative and so we have normalized them to the DWIA at $\phi = 10°$, at each respective total energy, in the $3p$ ground-state transition. Note that as, at each respective energy, relative normalizations are maintained in the binding-energy spectra this also sets, in each case, the absolute scale for all the other $3p^{-1}$ and $3s^{-1}$ satellites. Nearly all the $3p$ strength goes to the ground-state transition. This can be seen from Table I and is supported by the configuration-interaction (CI) calculations of Mitroy *et al.* [25]. We find in the present measurements that the spectroscopic factor for the $3p$ ground-state transition is 0.95 ± 0.01, and we have taken this value into account when normalizing the data. It is clear from Fig. 2 that to within the experimental uncertainties on the data, the DWIA provides an excellent description of the measured momentum distribution at each energy studied. At 1500 eV we can also compare the present measurement with the earlier one of McCar-

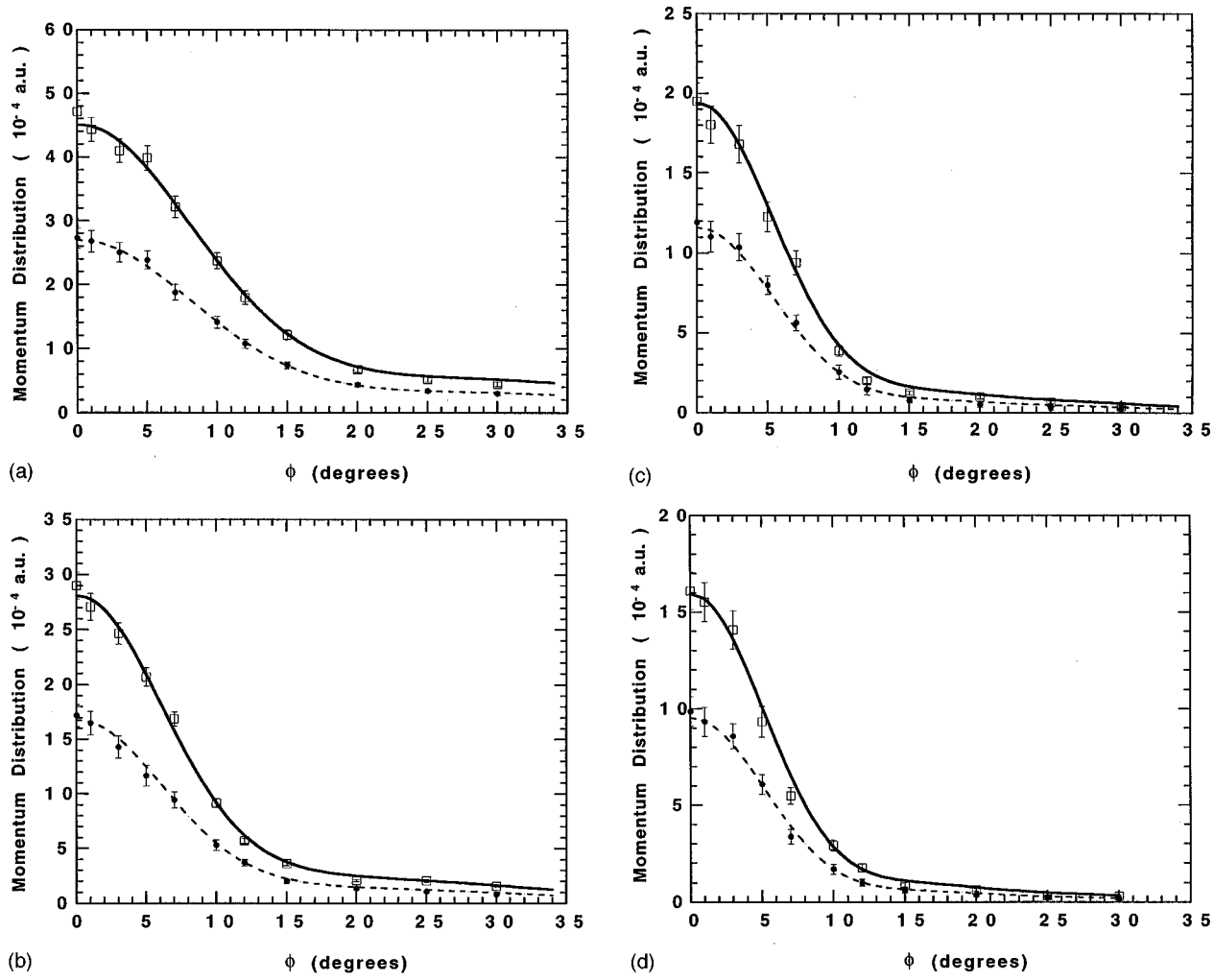

FIG. 3. Noncoplanar symmetric momentum distributions for the transition to the first excited $3s$ state ($\epsilon_i = 29.24$ eV) and total ^2S manifold, for $\epsilon_i \leq 45$ eV, at (a) 500, (b) 1000, (c) 1500, and (d) 1800 eV. The present data for the ''main'' transition at $\epsilon_i = 29.24$ eV (●), $0.55\times$DWIA (----), the present data for the ^2S manifold (□) and $0.92\times$DWIA (—) are plotted. Note the missing 8% ^2S manifold intensity for $\epsilon_i > 45$ eV, measured at 1000 eV, is consistent with the earlier result of McCarthy *et al.* [19].

thy *et al.* [19] [see Fig. 2(c)]. The level of agreement between them is quite good, except at the smaller values of ϕ where the effect of the different angular resolutions of the two experiments is most pronounced. We note the superiority of the present angular resolution over that employed in the earlier study [19]. While not specifically shown, the DWIA, when appropriately scaled, also provides a good description of the MDs for the other $3p^{-1}$ satellites (at $\epsilon_i = 35.60$, 37.15, and 39.56 eV, respectively) of the $^2P^o$ manifold. This is true for each of the energies of the present study. The current spectroscopic factors for states belonging to the $^2P^o$ manifold, at each energy studied and for representative values of recoil momentum (p or ϕ), are given in Table I. It is clear from this table that the values of these spectroscopic factors are independent of energy and momentum (ϕ) for all the $3p^{-1}$ transitions. It is also clear that the spectroscopic sum rule holds for all energy and momentum.

In Fig. 3 the present MD data for the $3s$ manifold and the main $3s^{-1}$ satellite, at $\epsilon_i = 29.24$ eV, are plotted at (a) 500, (b) 1000, (c) 1500, and (d) 1800 eV. Note McCarthy *et al.* [19] found that for binding energies in the range $45\,\text{eV} \leqslant \epsilon_i \leqslant 55\,\text{eV}$, which were not generally measured in this study, some 8% of the ^2S manifold cross section is to be found. This point was specifically checked by us at 1000 eV, in an independent measurement, and found to be correct. Hence in Fig. 3 the measured manifold MDs are compared against the $0.92\times$DWIA $3s$ result. No separate normalization of these data is allowed, since the measurements are normalized by the $3p^{-1}$ ground-state transition as discussed earlier. The $3s$ Hartree-Fock orbital of Clementi and Roetti [26] was used in these calculations to represent the Dyson orbital. It is apparent from this figure that both the shapes and magnitudes of the present MDs, at each energy investigated, are in excellent agreement, to within the experimental uncertainties, with the DWIA results. The shape of the measured $\epsilon_i = 29.24$-eV transition, also at each respective energy, is in good agreement with the results of the corresponding DWIA calculation, as is its magnitude, again at each energy, when the calculated manifold cross section is multiplied by the factor 0.55. This yields a consistent spectroscopic factor for this state of 0.55 (see Table II). While not actually illustrated, the DWIA, when appropriately scaled, also provides an excellent description of the MDs for the other $3s^{-1}$ transitions (at $\epsilon_i = 36.52$, 38.60, 41.21, 42.67, 43.4, 44.0, and 44.6 eV, respectively) of the ^2S manifold. This is the case for each of the total energies of the present study. McCarthy *et al.* [19] found it necessary to allow for a small $4s$ contribution to describe their measured MD at $\epsilon_i = 36.52$ eV, which is contrary to what we have found. However, we must note that there is quite a bit of scatter in those data [19] and the statistical quality of the $\epsilon_i = 36.52$-eV MD in the earlier work is also quite marginal. The current spectroscopic factors, at each energy studied and for representative values of recoil momentum (p or ϕ), for each of the satellites of the ^2S manifold are given in Table II. It is clear from this table that the values of these spectroscopic factors are independent of energy and momentum for all the $3s^{-1}$ transitions. It is also apparent from this table that if the 8% ^2S intensity in the binding energy range $45\ \text{eV} \leqslant \epsilon_f \leqslant 55$ eV is accounted for, the spectroscopic sum rule holds for all energy and momentum.

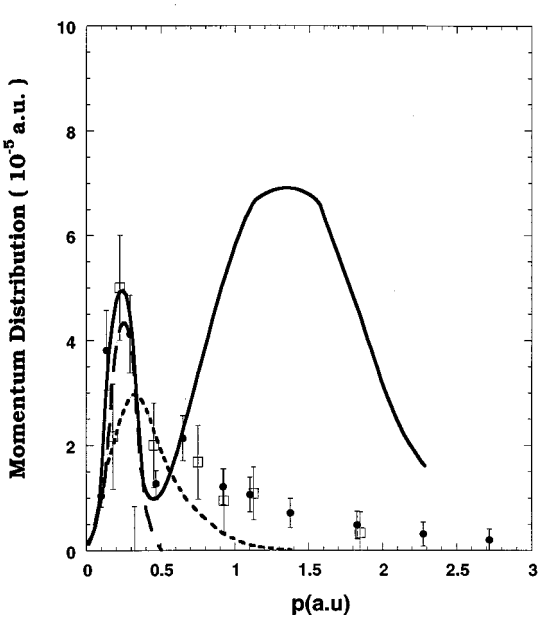

FIG. 4. 1500-eV noncoplanar symmetric momentum distribution for the transition to the $^2D^e$ state at $\epsilon_i = 34.20$ eV. The present data (●), the earlier result of McCarthy *et al.* (□), and DWIA results using $3d$ (--------) ($\times 0.01$) and $4d$ (--) ($\times 0.002$) Hartree-Fock [26] orbitals and the CI ($l=2$) wave function (—) ($\times 2$) of Mitroy *et al.* [25] are plotted for comparison.

Finally we briefly consider the MD for the state at binding energy 34.20 eV, which can only be excited through d-wave correlations in the ground state of the neutral argon atom. McCarthy *et al.* [19] measured a somewhat unusual momentum distribution which showed a primary maximum at $p \sim 0.25$ a.u., a minimum at $p \sim 0.4$ a.u., and a broad secondary maximum which peaked at $p \sim 0.7$ a.u. A CI ($l=2$) calculation from Mitroy *et al.* [25] qualitatively reproduced these features, although overestimating the strength at higher momenta, but there was still some concern that strongly overlapping wings from nearby states may have affected the MD they derived from their deconvolution process. As noted previously, with the improved energy resolution of the present study we largely avoid these concerns. The current MD result, at 1500 eV, for this ^2D state is given in Fig. 4. Also shown in this figure are the earlier measurements of McCarthy *et al.*, some DWIA results using $3d$ and $4d$ Hartree-Fock orbitals [26] multiplied by factors of 0.01 and 0.0002, respectively, and the result using the CI wave function from Mitroy *et al.* [25], multiplied by a factor of 2. Agreement between the present MD data and that of McCarthy *et al.* [19] is good, the present data being somewhat more accurate and exhibiting less scatter than the earlier work. The CI wave function of Mitroy *et al.* and the $4d$ Hartree-Fock wave function, both describe the low-momentum peak of this $^2D^e$ manifold transition, but the former seriously overestimates the high-momentum components whereas the latter has no higher momentum peak. Substantive agreement with theory therefore still awaits the development of a CI wave function which provides a better physical representation than that given in Mitroy *et al.* [25]. It is clear, since no d orbitals are occupied in the independent-particle model of the argon atom, that the magnitude and shape of this d-wave transition provides a very sensitive test of initial-state electron correla-

tion. Many-body calculations of the argon ground state are not yet capable of providing a full description of this *d*-wave correlation.

V. CONCLUSIONS

High-resolution binding-energy spectra over the valence region of argon were measured at four energies (500, 1000, 1500, and 1800 eV) and over a range of out-of-plane azimuthal angles ϕ (0°–30°). Momentum distributions were derived from these spectra, at each energy, for the $^2P^o$ and ^2S manifold cross sections and also for the individual transitions that constitute the respective manifold cross sections. On comparing these MD measurements with the corresponding results of DWIA calculations, using the $3p$ and $3s$ Hartree-Fock orbitals of Clementi and Roetti [26] to represent the Dyson orbital, substantive agreement between them is found in terms of both the shape and magnitude of the cross sections. Spectroscopic factors for the $3p^{-1}$ and $3s^{-1}$ satellites are derived and found to be independent of energy and momentum. The spectroscopic sum rule is also found to hold for both the $^2P^o$ and ^2S manifolds, relative to each other. Thus we conclude that we have unequivocally demonstrated that the three criteria of Sec. III, for experimental verification of the approximations of the EMS technique [Eq. (12)], have been met. Hence, in some sense, this study reports a definitive experiment for electron-momentum spectroscopy.

The energy- and momentum-independent $^2P^o$ and $^2S^e$ manifold spectroscopic factors provide a sensitive and rigorous test for the treatment of electron correlation effects in argon and its ion, particularly for final-state correlations. The observed shape and magnitude for the measured *d*-wave momentum profile to the ion state at $\epsilon_i = 34.20$ eV, with dominant configuration $3s^2 3p^4(^1D)4s\ ^2D$, provides a very sensitive test for initial-state correlations.

ACKNOWLEDGMENTS

This work was financially supported by the Australian Research Council (ARC). One of us (M.J.B.) also thanks the ARC for financial support.

[1] E. Weigold, S. T. Hood, and P. J. O. Teubner, Phys. Rev. Lett. **30**, 475 (1973).
[2] J. B. Furness and I. E. McCarthy, J. Phys. B **6**, L204 (1973).
[3] I. E. McCarthy and E. Weigold, Rep. Prog. Phys. **54**, 789 (1991).
[4] M. A. Coplan, J. H. Moore, and J. P. Doering, Rev. Mod. Phys. **66**, 985 (1994).
[5] J. J. Neville, Y. Zheng, B. P. Hollebone, N. M. Cann, C. E. Brion, C-K. Kim, and S. Wolfe, Can. J. Phys. **74**, 773 (1996).
[6] S. Svensson, K. Helenelund, and U. Gelius, Phys. Rev. Lett. **58**, 1624 (1987).
[7] M. Ya. Amusia and A. S. Kheifets, J. Phys. B **18**, L679 (1986).
[8] M. Ya. Amusia and A. S. Kheifets, Aust. J. Phys. **44**, 293 (1991).
[9] G. B. Hewitt, G. Cottrell, R. Northeast, S. Utteridge, and M. J. Brunger (unpublished).
[10] I. Bray and A. T. Stelbovics, Adv. At., Mol., Opt. Phys. **35**, 209 (1995).
[11] W. F. Ford, Phys. Rev. **133**, B1616 (1964).
[12] K. M. Watson, Rev. Mod. Phys. **30**, 565 (1958).
[13] P. J. Storer, S. A. C. Clark, R. C. Caprari, M. Vos, and E. Weigold, Rev. Sci. Instrum. **65**, 2214 (1994).
[14] S. F. Mazevet, I. E. McCarthy, and Y. Zhou, J. Phys. B **29**, L901 (1996).
[15] M. E. Casida and D. P. Chong, Int. J. Quantum Chem. **40**, 225 (1991).
[16] W. Kohn and L. J. Sham, Phys. Rev. **140**, A1133 (1965).
[17] W. von Niessen, J. Schirmer, and L. S. Cederbaum, Comput. Phys. Rep. **1**, 59 (1984).
[18] R. J. F. Nicolson, I. E. McCarthy, and M. J. Brunger. Aust. J. Phys. (to be published).
[19] I. E. McCarthy, R. Pascual, P. Storer, and E. Weigold, Phys. Rev. A **40**, 3041 (1989).
[20] S. T. Hood, I. E. McCarthy, P. J. O. Teubner, and E. Weigold, Phys. Rev. A **9**, 260 (1974).
[21] I. E. McCarthy and E. Weigold, Rep. Prog. Phys. **51**, 299 (1988).
[22] K. T. Leung and C. E. Brion, Chem. Phys. **82**, 87 (1983).
[23] J. F. Williams, J. Phys. B **11**, 2015 (1978).
[24] C. Moore, *Atomic Energy Levels*, Natl. Bur. Stand. (U.S.) Circ. No. 467 (U.S. GPO, Washington, DC, 1949), Vol. 1.
[25] J. D. Mitroy, K. A. Amos, and I. Morrison, J. Phys. B **17**, 1659 (1984).
[26] E. Clementi and C. Roetti, At. Data Nucl. Data Tables **14**, 177 (1974).